Journal of Power Sources 249 (2014) 118–124

Contents lists available at ScienceDirect

Journal of Power Sources

journal homepage: www.elsevier.com/locate/jpowsour

The design of a Li-ion full cell battery using a nano silicon and nano multi-layer graphene composite anode

KwangSup Eom [a,*], Tapesh Joshi [a], Arnaud Bordes [a], Inhwan Do [b], Thomas F. Fuller [a]

[a] School of Chemical & Biomolecular Engineering, Center for Innovative Fuel Cell and Battery Technologies, Georgia Institute of Technology, Atlanta, GA 30332, USA
[b] XG Sciences, Inc., 3101 Grand Oak Drive, Lansing, MI 48911, USA

HIGHLIGHTS

- Nano-Si and nano-graphene composite is used as an anode of Li-ion battery.
- This anode material shows high cyclability in half-cell and full-cell tests.
- The anode has a greater effect on the full-cell performance with NCA cathode.
- A FEC electrolyte additive improves the cyclability of the full cell.

ARTICLE INFO

Article history:
Received 24 July 2013
Received in revised form
18 October 2013
Accepted 21 October 2013
Available online 30 October 2013

Keywords:
Li ion battery
Full cell
Silicon–graphene composite
Nanosized graphene
Lithium nickel cobalt aluminum oxide cathode
Fluoro-ethylene carbonate

ABSTRACT

In this study, a Si–graphene composite, which is composed of nano Si particles and nano-sized multi-layer graphene particles, and micro-sized multi-layer graphene plate conductor, was used as the anode for Li-ion battery. The Si–graphene electrode showed the high capacity and stable cyclability at charge/discharge rate of C/2 in half cell tests. Nickel cobalt aluminum material (NCA) was used as a cathode in the full cell to evaluate the practicality of the new Si–graphene material. Although the Si–graphene anode has more capacity than the NCA cathode in this designed full cell, the Si–graphene anode had a greater effect on the full-cell performance due to its large initial irreversible capacity loss and continuous SEI formation during cycling. When fluoro-ethylene carbonate was added to the electrolyte, the cyclability of the full cell was much improved due to less SEI formation, which was confirmed by the decreases in the 1st irreversible capacity loss, overpotential for the 1st lithiation, and the resistance of the SEI.

1. Introduction

Li-ion batteries (LIBs) have been widely used as an energy storage system for various electrical devices from small consumer electronics to electrical vehicles (EVs) due to their stable long-term performance (cyclability), good rate capability, and thermal stability in practical use [1–3]. However, one of the most critical challenges of present commercial Li-ion batteries is their insufficient capacity leading to a need for frequent charging. Hence, development of new electrode materials with higher energy density is of significant interest [3]. Silicon is a promising anode material due to its high theoretical specific capacitance (4200 mAh g^{-1}) [4–19]. Unfortunately, Si expands up to 300% during lithiation, resulting in a large irreversible capacity loss (ICL). To mitigate this capacity fade, nanowire-shaped Si [4,5] with good flexibility and Si composites with buffer materials, such as pre-treated carbon [6–8] and various shaped (sized) graphenes [9–18] have been used. Graphene has received a lot of attention because it has high electrical conductivity as well as high mechanical strength, resulting in the simultaneous increase in rate capability and cycle life for the Si–graphene electrode. In order to take full advantage of the two positive effects of graphene, the size and composition of Si and graphene must be optimized. In this study, we used a Si–graphene electrode that was fabricated with the active materials (nano-sized Si (<100 nm) and multi-layer graphene plates (<100 nm)) and conducting additive (micro-sized multi-layer graphene plate).

* Corresponding author. Tel.: +1 404 747 0451.
E-mail addresses: keom@gatech.edu, kwangsup.eom@gmail.com (K. Eom).

0378-7753/$ – see front matter © 2013 Elsevier B.V. All rights reserved.
http://dx.doi.org/10.1016/j.jpowsour.2013.10.087

Although there are many reports on Si–graphene anode materials, most of the data are from half-cell tests [9–18]. In practice, the electrochemical behavior of a half cell is different from that of a full cell. It was reported that the full cells employing nano Si–graphene anodes with cathodes such as $LiNi_{1/3}Co_{1/3}Mn_{1/3}$ (NCM) [14] and $Li_{1.2}Ni_{0.2}Mn_{0.6}O_2$ (LNM) [18] showed lower capacity and greater capacity fade than the individual Si–graphene half cells. These full-cell studies did not report the active material ratio for the electrodes. Consequently, it is difficult to ascribe a cause for the greater capacity fade in full cells. The lower performance might be due to the limited supply of cyclable lithium provided by the positive electrode, an increase in resistance of components by additional SEI formation, or dissolution of electrolyte and metals from the cathode. Accordingly, in order to estimate the feasibility for a practical use of a new material, a full cell is necessary.

Herein, we designed the Li-ion full cell employing a new nano Si–graphene composite anode with an NCA cathode and investigated its electrochemical and microstructural behaviors during charge/discharge cycling. To improve further cyclability, fluoroethylene carbonate (FEC) was added to the EC–DEC electrolyte, and its effect was explored electrochemically.

2. Experimental methods

2.1. Material preparation

A commercially available Si–graphene composite (*XG-SiG*™, supplied by *XG Sciences, Inc.*) was used for the anode. The active material was composed of nano Si particles and nano-sized plate-like multi-layer graphene (*xGnP*®). To make the slurry of adhesive and conductive anode material, the nano-sized active material was combined with polyacrylic acid (PAA) binder (*Sigma Aldrich*, M_v: 450,000 g mol^{-1}), carbon black conductive agent, and conductive additive of micro-sized multi-layer granular graphene (*xGnP*®) with very high conductivity of 10^7 S m^{-1}, and PGME solvent (Propyleneglycol monomethyl ether, *Sigma Aldrich*). After mixing the slurry by sonication and stirring with magnetic bar in a jar, the slurry was coated on a 10 μm Cu foil using a doctor blade. The slurry coated on Cu foil was dried for 1 h at a room temperature and then in a vacuum oven of 80 °C for overnight. The active loading was between 1.64 and 1.66 mg cm^{-2}. The theoretical capacity was calculated to 2968 mAh g^{-1} based on the individual theoretical capacities of Si and carbon materials (Si: 4200 mAh g^{-1}, Carbon: 372 mAh g^{-1}).

The density of material was between 0.63 and 0.70 g cm^{-3} without calendaring. An active material of NCA was used for a cathode with a graphitic carbon conductive additive and polyvinylidenefluoride (PVdF) binder.

2.2. Cell assembly and electrochemical properties

All half cells were assembled as 2032 coin cells, and all full cells were fabricated as pouch-type cells with an active area of 9 cm^2. The composition of electrolyte was EC: DEC = 1:1 (w/w) with 1 M $LiPF_6$ with/without 10 wt.% FEC. The loadings of active material (anode:cathode) were 0.00263 g:0.0230 g and 0.0141 g:0.131 g in a coin and pouch cell, respectively. Hence, the design capacity of anode and cathode based on the theoretical capacity (Si–graphene anode of 2968 mAh g^{-1} and NCA cathode of 274 mAh g^{-1}) was 7.80 and 6.38 mAh for coin cells, respectively; that is, the theoretical capacity of the anode was 1.22 times more than that of cathode. Using the measured capacity after the 1st formation cycle for the half cells, the lithiation capacity of Si–graphene anode is 4.46 mAh (1696 mAh g^{-1}) and the delithiation capacity of NCA cathode is 3.83 mAh (169 mAh g^{-1}) for coin cells, indicating that the design capacity of anode is 1.16 times more than that of cathode. To see both effects of anode and cathode on the capacity fade of the full cell during cycling, the capacity ratio of anode: cathode was designed to be close to 1:1.

To characterize the electrochemical properties of the full cells, capacity–voltage (*C–V*) tests were performed at various C-rates (C/15 for 1st 5 cycles, C/5 for 2nd 5 cycles, and C/2 for subsequent cycle), which were determined from the capacity of cathode on the 1st cycle. All cycling tests were conducted at room temperature (20 °C) using an *Arbin* battery cycler. The full cells were charged to 4.2 V at constant current (CC), and then held at a constant voltage (CV) until the current was half of applied C-rate (C/30, C/10, and C/4). Discharges were done at CC to a cut-off potential of 2.75 V. The capacities of full cells were normalized by the weight of NCA cathode. The half cells were cycled between 0.05 and 1.0 $V_{Li+/Li}$ (Si/graphene) and 2.75–4.20 $V_{Li+/Li}$ (NCA). Electrochemical Impedance Spectroscopy (EIS) of full cells was conducted using a potentiostat in a frequency range of 1 MHz ~ 0.01 Hz with an amplitude of 5 mV at full state of charge (SOC) of 4.09–4.12 V. The values for resistances of individual components were determined with a fitting program.

2.3. Surface and microstructural analysis of electrode

The surface morphologies and compositions of electrode materials were analyzed by a high resolution scanning electron microscopy (SEM, *Hitachi SU8000*). The atomic composition was analyzed by energy dispersive spectroscopy (EDS). The microstructure of nano-sized Si and graphene composite was analyzed by a transmission electron microscopy (TEM) and X-ray diffraction (XRD).

3. Results and discussion

3.1. Nano-Si and nano-graphene composite for Li-ion battery anode

Fig. 1a shows the HR–SEM surface morphology, TEM bright field images, and XRD patterns of the as-prepared electrode of nano Si–graphene composite coated on a Cu foil. As shown in Fig. 1a–b, the electrode is composed of micro-sized graphene plates (diameter: 0.4–1 μm) and many spherical agglomerates of nano-sized particles composed of Si and graphene. Specifically, it is confirmed that the sizes of graphene plate particles are between 40 and 70 nm from the high magnification images (below) of Fig. 1a and the diameter of spherical Si is between 10 and 80 nm from TEM images (black dots and their agglomerates) of Fig. 1b. The TEM diffraction pattern of the Si–graphene electrode coated on Cu film shows the poly-crystalline ring and halo indicating an amorphous structure, which is probably due to activated carbon black. In particular, it was found from the XRD pattern of Fig. 1c that in the as-prepared electrode, the Si has poly-crystalline structure with sharp Si (111), Si (220), and Si (311) peaks, and the carbon materials show features of both an amorphous phase and a crystalline phase with graphitic C (002) and small C (004) peaks due to activated carbon black and multi-layer graphene plates in nano- and micro-scale.

Fig. 2a–b displays voltage–capacity curves and the corresponding differential curves showing the lithiation and delithiation behavior of half cells of Si–graphene, respectively. For the first cycle (C/15), the half cell of the Si–graphene composite showed the initial irreversible capacity loss (ICL) of 19.9% (CE of 80.1%) from 2782 to 2227 mAh g^{-1}, which is considerably improved value when compared with those from previous reports (27% [9], 30% [11], 37% [12], 23.1% [16], 22.6% [18], and 20–30% [10,13,15,17]). Recently, one Si–carbon composite material reported a very high 1st coulombic efficiency of 86% [19], however, the values of most Si–carbon/

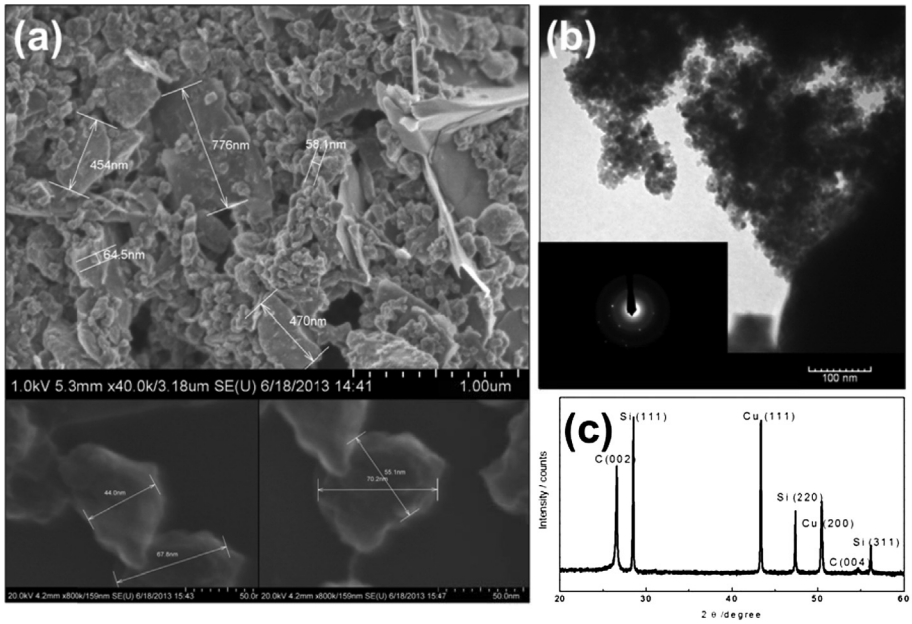

Fig. 1. (a) High-resolution SEM images, (b) TEM bright field images, diffraction pattern, and (c) XRD patterns of the as-prepared nano Si-nano graphene composite electrode.

graphene materials has been reported to be lower than 80% [9–13,15–18]. Starting with the 2nd cycle, the half cell was lithiated and delithiated at the C/2 rate. The delithiation capacity decreased from 1637 to 1116 mAh g^{-1}, but the capacity for the 6th cycle increased slightly to 1258 mAh g^{-1}. The capacity varied between 1069 and 1288 mAh g^{-1} out to the 30th cycle as shown in Fig. 2c. Afterward, the capacity decreased a little to 984–1088 mAh g^{-1}, but showed a stable behavior even at high charge/discharge rate of C/2, where the coulombic efficiency (CE) was between 98.9 and 99.4%. This improvement of the new Si–graphene composite electrode in

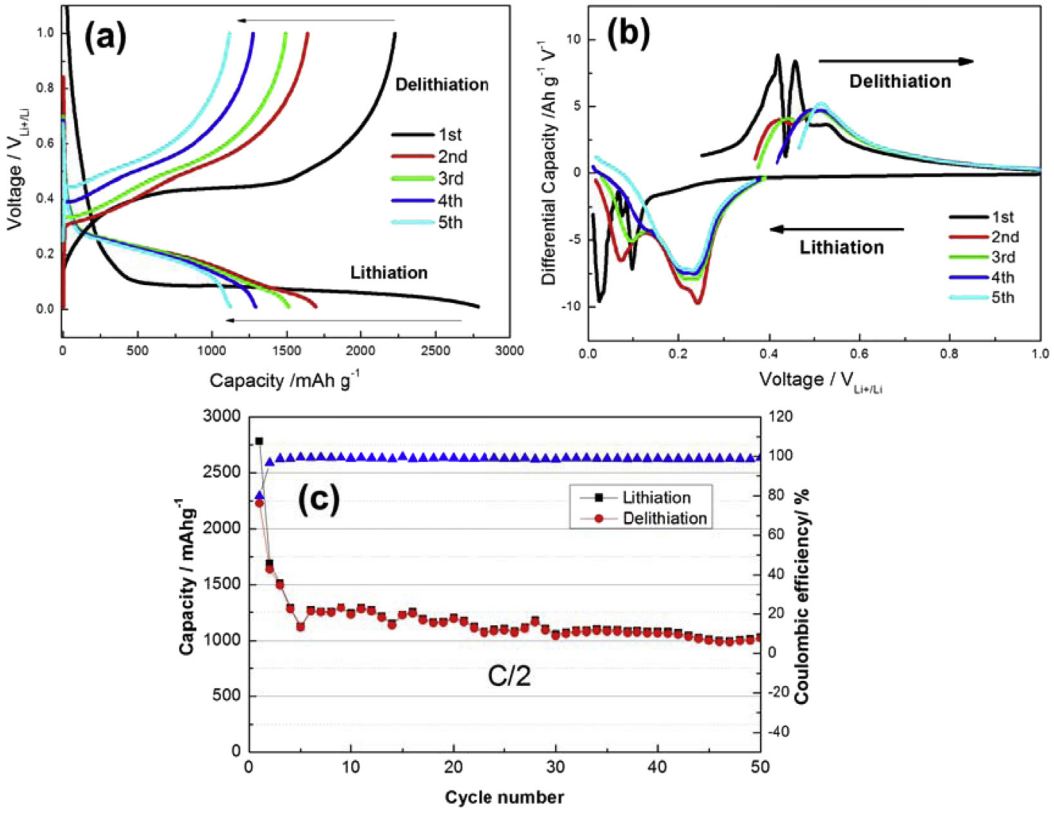

Fig. 2. (a) Voltage–capacity curves, (b) corresponding differential capacity curves, and (c) capacity fade of the half cell employing nano Si–graphene electrode between 0.05 and 1.0 $V_{Li+/Li}$ at C/2 (C/15 for the 1st cycle).

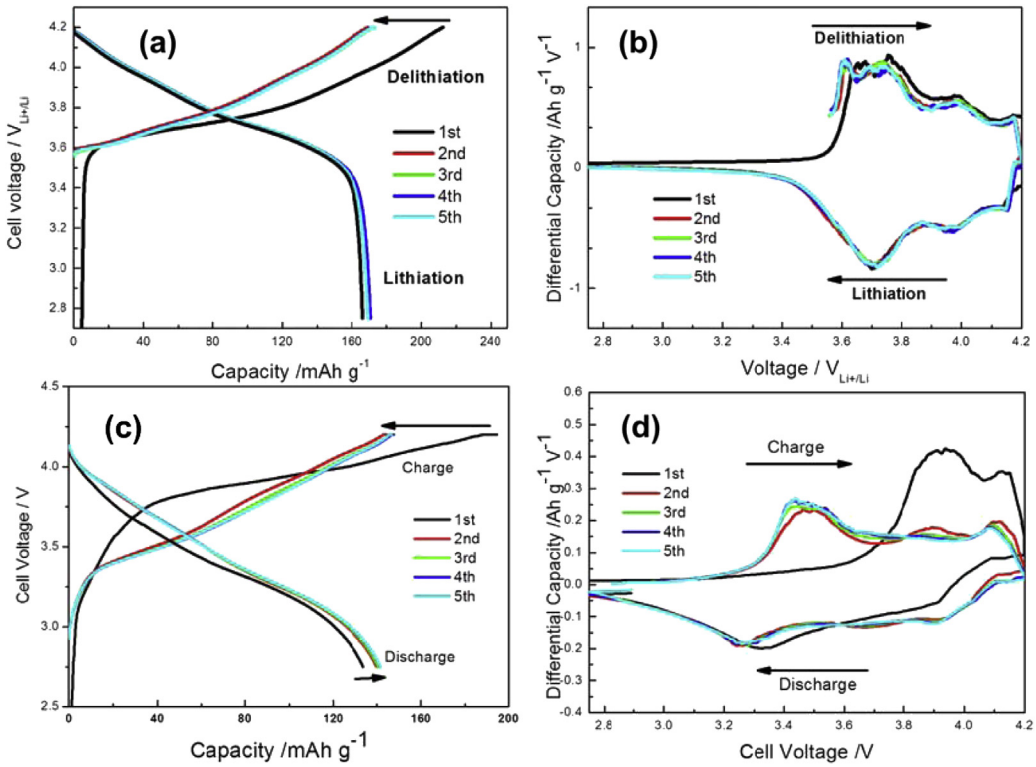

Fig. 3. (a) Voltage–capacity curves and (b) corresponding differential capacity curves of the half cell employing NCA electrode between 2.75 and 4.2 $V_{Li+/Li}$ at C/15. (c) Voltage–capacity curves and (d) corresponding differential capacity curves of the full cell employing nano Si–graphene anode and NCA cathode between 2.75 and 4.2 V_{cell} at C/15.

term of cyclability and kinetics is likely due to a buffering effect attributed to the nano-sized multi-layer graphene particles and lower electrode resistance due to the highly conductive multi-layer graphene additive.

In the *dC*/*dV* curves of Fig. 2b, it was confirmed that the Si–graphene electrode showed a significantly different behavior between the 1st and subsequent cycles. Specifically, the lithiation peaks at 0.02 and 0.1 V shown during 1st cycling disappeared, and

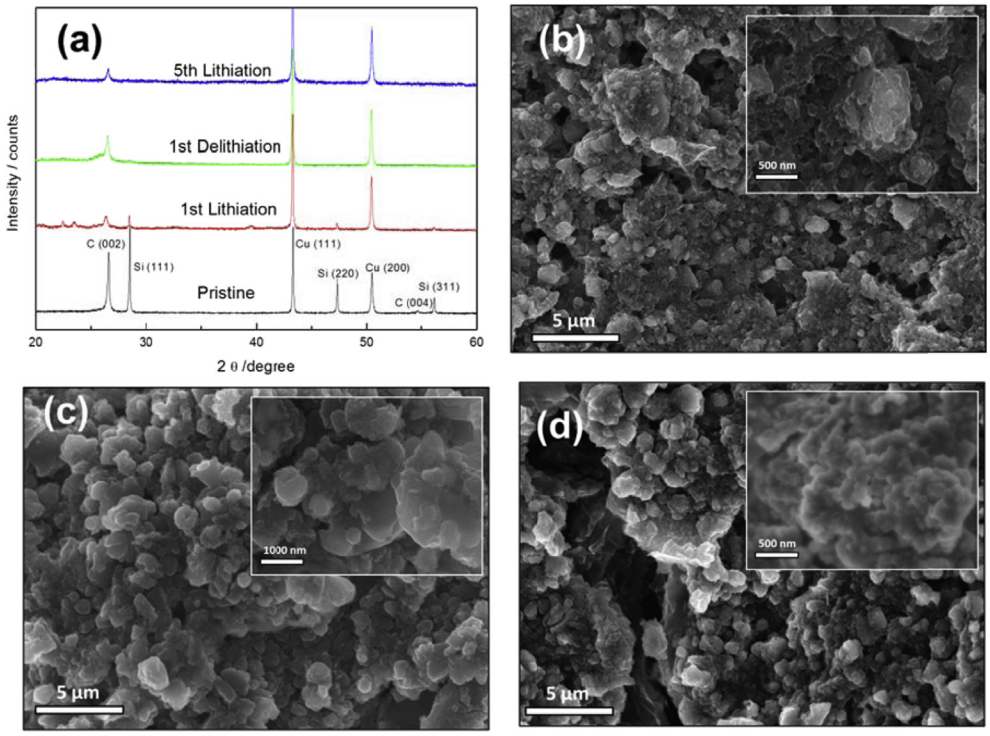

Fig. 4. (a) XRD patterns and SEM surface morphologies of Si–graphene electrode (b) before and after (c) the 1st lithiation, and (d) the 1st delithiation in the full cell test (cathode: NCA).

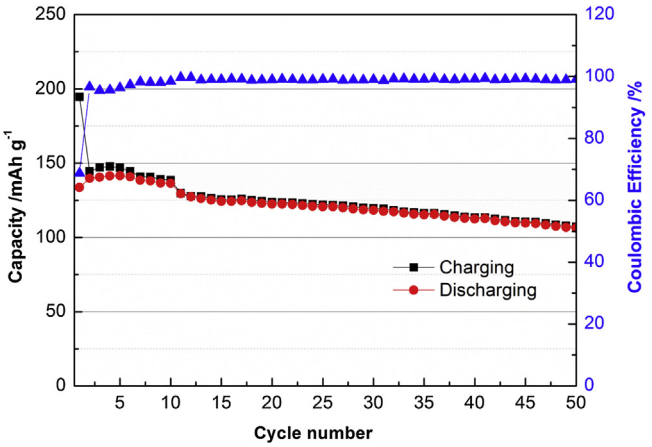

Fig. 5. Capacity fade of a pouch full cell using a Si–graphene anode and NCA cathode at C-rates of C/15 in 1st ~ 5th, C/5 in 5th ~ 10th, and C/2 in 10th ~ 50th in the electrolyte of EC: DEC = 1:1 (w/w) with 1 M $LiPF_6$.

new peaks were formed at 0.08, 0.20, and 0.24 V. Subsequently, the peak at 0.08 V decreased slightly and disappeared after the 5th cycle. According to the previous results [5,6,18], it is suggested that this behavior is attributed to the phase transformation of Si from crystalline to amorphous.

3.2. Design of the full cell employing Si–graphene and NCA electrode

Fig. 3a shows voltage–capacity curves of the NCA half cell, which was tested between 2.75 and 4.20 $V_{Li+/Li}$ at constant current (CC) of C/15. The corresponding differential capacities are presented in Fig. 3b. Except for the 1st delithiation, it was found that the capacity and lithiation/delithiation behavior of the NCA electrode was unchanged in both curves of Fig. 3a–b. It indicates that a lithiation/delithiation process is stable without a specific phase transformation with cycling. This NCA electrode was used as a cathode in the full cell for the practical test of the new Si–graphene composite anode. Fig. 3c shows the charging/discharging curves of a full pouch cell at C/15. The full cell showed no capacity fading between 1st and 5th cycles except for the large irreversible capacity loss (ICL) associated with the first charge. The initial discharge capacity based on weight of cathode is 133 mAh g^{-1}, which is lower than that of the NCA half cell (169 mAh g^{-1}) even though anode capacity is designed to be 1.16 times more than that of the cathode based on actual initial capacities of each electrode (the 1st cycled capacity of anode and cathode were 4.46 and 3.83 mAh in the each half coin cell). It might be due to unstable interfaces between both electrodes and electrolyte, and an increase in overall resistances through the cell. After the 1st cycle, the discharge capacity increased to 140 mAh g^{-1} and then remained constant through five cycles. After five cycles, from Figs. 2a and 3a, the capacity of the Si–graphene anode decreased from 4.46 to 3.13 mAh, whereas the capacity of cathode changed only slightly from 3.83 to 3.89 mAh. That is, the capacity ratio of anode over cathode decreased from 1.16 to 0.80. This decrease means that the capacity of the full cell is determined by the capacity of anode after five cycles.

Fig. 3d shows *dC*/*dV* behaviors with cycling, which are obtained from the data in Fig. 3c. Specifically, it is notable that the 1st electrochemical lithiation behavior is significantly different from that of subsequent cycles. During the subsequent charging, a large broad peak presented at 3.9 V was decreased dramatically and disappeared after the 2nd cycling. The second peak shown at 4.1 V decreased significantly after 1st cycling, and the new broad peak produced at 3.4 V and remained constant with cycling. This behavior is similar to the lithiation of the Si–graphene half cell, but differs from delithiation of the NCA half cell.

From the XRD patterns of Fig. 4a, it is confirmed that crystalline Si was largely changed to amorphous after the 1st charge and altered perfectly amorphous after the 1st discharge. Hence, it is considered that the *dC*/*dV* peak (Fig. 3d) of 3.9 V presented during 1st lithiation and the new peak produced at 3.4 V produced after the 2nd cycle are attributed to the reaction of Li ion with crystalline Si and amorphous Si, respectively. The second peak at 4.1 V is due to multi-layer graphene lithiation, the peak decreased after the 1st cycle, the intensity remained constant during subsequent cycling, and the XRD peak of graphitic (002) peak still remained after the 1st delithiation and the 5th lithiation.

Fig. 4b–d shows the SEM surface morphology of Si–graphene anode before and after the 1st lithiation and the 1st delithiation. After the 1st lithiation (Fig. 4c), due to Si expansion by lithiation the diameter of the spherical particles agglomerated with nano Si and nano multi-layer graphene particles is more than 2 times larger than that of the pristine Si–graphene (Fig. 4b). After the 1st delithiation (Fig. 4d), the particle size decreased, but cracks of 5 μm in width were seen on the surface. However, the morphology did not return to pristine state most likely because of SEI and crack formation between particles during the 1st lithiation and delithiation, resulting in an initial large irreversible capacity loss (ICL).

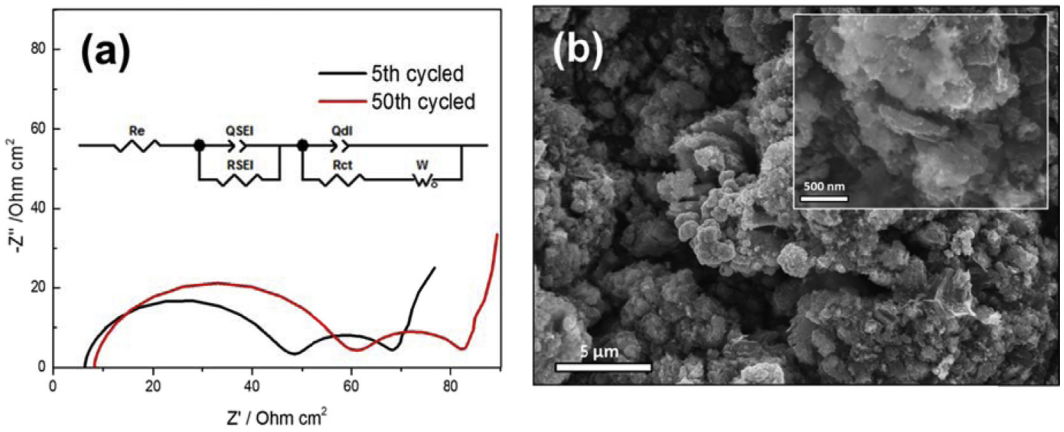

Fig. 6. (a) The EIS Nyquist plots of the full cell employing Si–graphene anode and NCA cathode after the 5th and 50th cycle in a frequency range of 1 MHz ~ 0.01 Hz with an amplitude of 5 mV at full state of charge (SOC) of 4.09–4.12 V (b) SEM surface morphologies of Si-graphene electrode after the 50th lithiation in the full cell.

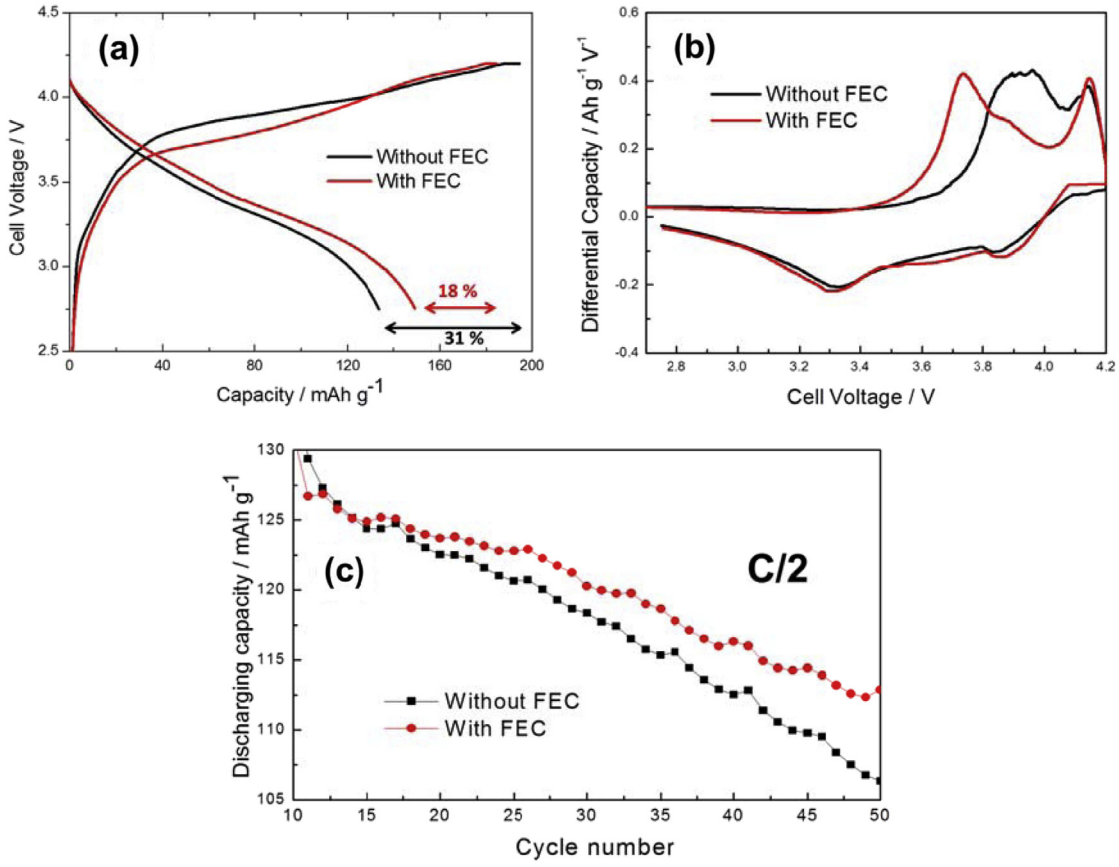

Fig. 7. Effect of the addition of FEC (10 wt.%) in EC: DEC electrolyte (1:1 wt.%) with 1 M $LiPF_6$ on (a) the first charging/discharging curves (at C/15), (b) the corresponding first differential curves, and (c) capacity fade (between 2.75 and 4.2 V at C/2) of pouch full cells employing Si–graphene anode and NCA cathode during 50 cycles.

3.3. *Capacity fade and degradation mechanism of the full cell*

Fig. 5 shows the capacity fade (cyclability) of the full cell at C/15 (1st ~ 5th), C/5 (6th ~ 10th), and C/2 (11th ~ 50th) cycles. With initial cycling, the capacity decreased very slightly and the coulombic efficiency (CE) increased, stabilizing at 98.9–99.5% after ten cycles. Nevertheless, the capacity decreased gradually from 129 to 107 mAh g^{-1} at C/2 from 10th to 50th cycles. It might be due to the break-up of Si particles and continuous formation of SEI layer on newly exposed surface of pulverized Si.

This hypothesis is supported by changes in the EIS (Fig. 6a) and surface morphology (Fig. 6b) after the 50th cycling. As shown in Fig. 6a, a Nyquist plot for the full cell consists of a high-frequency Z_{im}-intercept, first high-frequency semi-circle, the second middle-frequency semi-circle, and low-frequency curve, which are attributed to the resistances of electrolyte, the SEI films (mostly on anode), the charge-transfer resistance, and diffusion in electrodes, respectively [20,21]. Between the 5th and 50th cycles, the resistance of SEI increased by 27% (11.3 Ω cm^2) whereas the other resistances were largely unchanged. In the SEM surface images of a

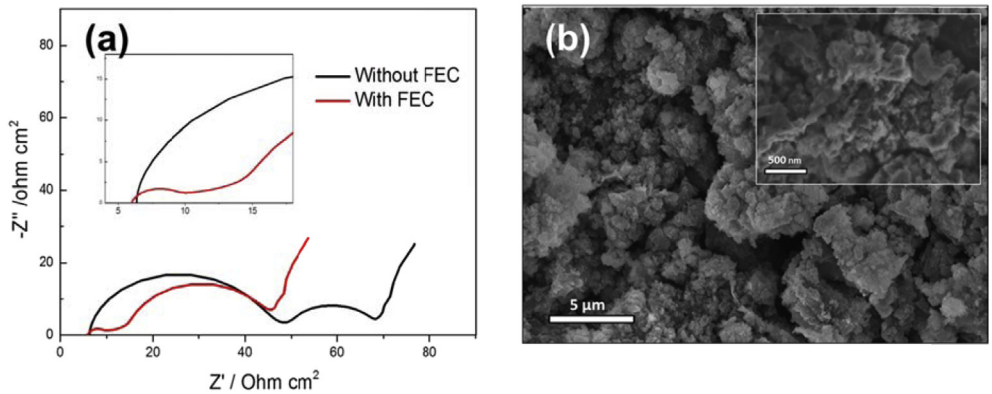

Fig. 8. Effect of the addition of FEC (10 wt.%) in EC: DEC electrolyte (1:1 wt.%) with 1 M $LiPF_6$ on the (a) EIS Nyquist plots measured after 5th formation cycles at fully charged state of the full cell employing Si–graphene anode and NCA cathode, and (b) SEM surface morphology of Si–graphene electrode after the 50th cycling.

lithiated anode after the 50th cycle (Fig. 6b), particles, less than 10 nm, are evident. These very small particles are probably due to Si pulverization during cycling. An abundance of SEI-like layer covered the surface of the anode randomly, which is clearly different from that of the 1st lithiation state of Fig. 4c. Hence, it was thought that a decrease in SEI formation would be able to increase the cyclability of full cells. According to previous reports [22–24], FEC is a good additive to improve the cyclability by reducing SEI formation by decreasing the reduction rate of electrolyte especially at the anode.

3.4. Effects of FEC on the capacity fade of full cell

Fig. 7a–b presents the effects of FEC additive on the 1st charging/discharging behavior and differential capacity of the full cells. The irreversible capacity loss (ICL) decreased dramatically from 31% to 18%, and the overpotential for the 1st lithiation decreased about 0.2 V, indicating that Li ion can diffuse more easily into anode probably due to less SEI formation with the FEC additive. The cyclability was improved as shown in Fig. 7c. In particular, the difference of discharge capacity increased with cycling, and at 50th cycles that of cells with FEC is 9.4% higher than that without FEC. The above data agree with the results of EIS curves of Fig. 8a and SEM surface images of Fig. 8b. With the addition of FEC, the diameter of high frequency semi-circle regarded as SEI film resistance decreased significantly from 40.5 to 4.5 $\Omega\ cm^2$. Moreover, the bright and rough SEI-like layers observed in Fig. 6b decreased clearly as shown in Fig. 8b.

For more improvement of the cyclability of this full cell, the effects of FEC additive on the electrochemical and microstructural changes of each component of Si–graphene anode, NCA cathode, and electrolyte should be studied with optimization of FEC contents. This work was prepared as the 2nd paper that continues this work.

4. Conclusions

The Si–graphene composite anode used in this study was composed of nano-sized Si particles and nano-sized multi-layer graphene plates, and micro-sized multi-layer graphene plate conductor, and showed stable cyclability and high capacity of more than 1000 mAh g^{-1} at high charge/discharge rate of C/2. The NCA was used as a cathode in design of the full cell to test the feasibility of a practical use of the new Si–graphene composite anode. The electrochemical and microstructural behaviors of the full cell during charge/discharge cycling were investigated. Although the Si–graphene anode has more capacity than the NCA cathode in this full cell, the cell performance was affected more significantly by the Si–graphene anode than the NCA cathode during cycling. A continuous decrease in capacity during cycling was due to the continuous SEI formation and pulverization of Si on anode, which was confirmed by EIS and SEM analyses. Hence, to improve the cyclability of the full cell through less SEI formation, a fluoro-ethylene carbonate (FEC) was added to the EC–DEC electrolyte. The cyclability of the full cell was improved, which is confirmed by decreases in irreversible capacity and overpotential for the 1st lithiation, and the resistance of SEI.

Acknowledgments

This research was supported by the U.S. Department of Energy SBIR Program and ‘ National Research Foundation of Korea (2012R1A6A3A03040261)’.

References

[1] M.S. Whittingham, Chem. Rev. 104 (2004) 4271–4302.
[2] M. Armand, J.M. Tarascon, Nature 451 (2008) 652–657.
[3] V. Etacheri, R. Marom, R. Elazari, G. Salitra, D. Aurbach, Energy Environ Sci. 4 (2011) 3243–3262.
[4] C.K. Chan, H. Peng, G. Liu, K. McIlwrath, X.F. Zhang, R.A. Huggins, Y. Cui, Nat. Nanotechnol. 3 (2008) 31–35.
[5] M. Ge, J. Rong, X. Fang, C. Zhou, Nano Lett. 12 (2012) 2318–2323.
[6] M.K. Datta, P.N. Kumta, J. Power Sources 158 (2006) 557–563.
[7] A. Magasinski, P. Dixon, B. Hertzberg, A. Kvit, J. Ayala, G. Yushin, Nat. Mater. 9 (2010) 353–358.
[8] X. Feng, J. Yang, P. Gao, J. Wang, Y. Nuli, RSC Adv. 2 (2012) 5701–5706.
[9] S.-L. Chou, J.-Z. Wang, M. Choucair, H.-K. Liu, J.A. Stride, S.-X. Dou, Electrochem. Commun. 12 (2010) 303–306.
[10] J.K. Lee, K.B. Smith, C.M. Hayner, H.H. Kung, Chem. Commun. 46 (2010) 2025–2027.
[11] Y.S. He, P.F. Gao, J. Chen, X.W. Yang, X.Z. Liao, J. Yang, Z.F. Ma, RSC Adv. 1 (2011) 958–960.
[12] H.-C. Tao, L.-Z. Fan, Y. Mei, X. Qu, Electrochem. Commun. 13 (2011) 1332–1335.
[13] X. Zhao, C.M. Hayner, M.C. Kung, H.H. Kung, Adv. Energy Mater. 1 (2011) 1079–1084.
[14] L. Ji, H. Zheng, A. Ismach, Z. Tan, S. Xun, E. Lin, V. Battaglia, V. Srinivasan, Y. Zhang, Nano Energy 1 (2012) 164–171.
[15] X. Xin, X. Zhou, F. Wang, X. Yao, X. Xu, Y. Zhu, Z. Liu, J. Mater. Chem. 22 (2012) 7724–7730.
[16] X. Zhou, A.-M. Cao, L.-J. Wan, Y.-G. Guo, Nano Res. 5 (2012) 845–853.
[17] Y. Zhu, W. Liu, X. Zhang, J. He, J. Chen, Y. Wang, T. Cao, Langmuir 29 (2012) 744–749.
[18] J.-G. Ren, Q.-H. Wu, G. Hong, W.-J. Zhang, H. Wu, K. Amine, J. Yang, S.-T. Lee, Energy Technol. 1 (2013) 77–84.
[19] S. Iwamura, H. Nishihara, T. Kyotani, J. Power Sources 222 (2013) 400–409.
[20] S.S. Zhang, K. Xu, T.R. Jow, Electrochim. Acta 49 (2004) 1057–1061.
[21] L. Chen, K. Wang, X. Xie, J. Xie, J. Power Sources 174 (2007) 538–543.
[22] V. Etacheri, O. Haik, Y. Goffer, G.A. Roberts, I.C. Stefan, R. Fasching, D. Aurbach, Langmuir 28 (2011) 965–976.
[23] H. Nakai, T. Kubota, A. Kita, A. Kawashima, J. Electrochem. Soc. 158 (2011) A798–A801.
[24] Y.-M. Lin, K.C. Klavetter, P.R. Abel, N.C. Davy, J.L. Snider, A. Heller, C.B. Mullins, Chem. Commun. 48 (2012) 7268–7270.